Dynamic weakening by nanoscale smoothing during high-velocity fault slip

Xiaofeng Chen[1], Andrew S. Madden[1], Barry R. Bickmore[2], and Ze'ev Reches[1]*
[1]School of Geology and Geophysics, University of Oklahoma, Norman, Oklahoma 73019, USA
[2]Department of Geological Sciences, Brigham Young University, Provo, Utah 84602, USA

ABSTRACT

Slip during large earthquakes occurs along faults that are hundreds of kilometers long, yet the dynamic weakening that drives these earthquakes is controlled by nano- to micro-scale frictional processes. We analyzed these processes along experimental faults that slipped at rates approaching seismic velocity, and which displayed intense dynamic weakening of 50%–70%. Sheared fault surfaces were extracted, and then atomic force microscopy was used to (1) measure friction on a sub-micron scale, and (2) determine the three-dimensional morphology at the nano- to micro-scale. The sheared surfaces developed a prevalent anisotropy with a weaker and smoother axis along the slip direction. The nanoscale friction coefficient correlates well with sheared-surface roughness: the friction coefficients dropped only on surfaces with root mean square (RMS) values of <100 nm, while rougher surfaces showed no weakening. Our analysis indicates that slip smoothing at high slip velocities can be an effective mechanism of dynamic weakening.

INTRODUCTION

Rock friction, which has profound effects on faulting processes and earthquake instability, has been studied in numerous experiments (Tullis, 1996; Byerlee, 1978; Scholz, 1998). However, the typical experimental analyses suffer from a major inconsistency. On one hand, the rock friction is commonly determined through measurements on relatively large rock samples, with areas from a few square centimeters to 1 m^2 (Byerlee, 1978; Lockner and Okubo, 1983); but on the other hand, theoretical models of frictional processes are scale dependent (Li and Kim, 2008), and active at small scales of a few microns or less (Carpick et al., 1996; Mo et al., 2009; Li et al., 2011). Small-scale friction processes include asperity failure and deformation (Byerlee, 1967; Dieterich and Kilgore, 1994), gouge lubrication (Reches and Lockner, 2010), shearing of clays (Moore and Rymer, 2007), melting (Tsutsumi and Shimamoto, 1997), and flash heating (Goldsby and Tullis, 2011). In the present study, we eliminate this inconsistency by direct friction analysis from nano to macro scales.

We conducted rock friction experiments on experimental fault surfaces that were sheared at high slip velocity up to 0.9 m/s (approximate seismic slip velocity) under normal stress up to 7.0 MPa (Reches and Lockner, 2010). We used atomic force microscopy (AFM) and scanning electron microscopy to determine the frictional strength and roughness of the fault surfaces, and link these results to the macroscopic experimental observations.

METHODS AND MATERIALS

We measured the friction coefficient on experimental faults made of Sierra White granite (SWG) from California and Kasota dolomite (KD) from Minnesota, United States (see the GSA Data Repository[1]). The experimental faults were sheared by a rotary apparatus, in which two rock blocks with a ring-shaped contact slipped with respect to each other (Reches and Lockner, 2010; Fig. DR1 in the Data Repository). The sheared fault surfaces displayed slickenside striations parallel to the slip direction that resemble the well-known striations along natural faults (Fig. 1). Parts of the fault surfaces developed a light-reflective, hard coating (Fig. 1B) similar to that in previous observations (Han et al., 2007; Smith et al., 2012).

We used two modes of AFM operation. The micron-scale morphology of the fault surfaces was measured in the intermittent contact mode that uses a sharp probe mounted on the end of a flexible cantilever (Maurice and Lower, 2008) (see the Data Repository). The friction coefficient (FC), μ = (shear force) / (normal force), was measured by using the axial method (Stiernstedt et al., 2005; Attard et al., 2007; Kosoglu et al., 2010) in which a spherical silica glass bead (tens of microns in diameter) replaces the sharp tip on the cantilever (Fig. DR3). The FC is calculated from the hysteresis of the deflection of the cantilever while the probe, in contact with the sample, is advanced and retracted along the surface (see the Data Repository). The axial method provides friction data for length scales of 0.1–0.25 μm, and allows for many measurements at the same spot under dry or

wet conditions. This method yielded FC values in good agreement with macroscopic friction measurements for Na-montmorillonite samples (Kosoglu et al., 2010).

The FC was measured with AFM by aligning the cantilever's long axis either parallel or normal to the slickenside striations. We measured FC at 43 sites on our samples, and the measurement was repeated hundreds of times at each site (Table DR1 in the Data Repository). The average standard deviation in the FC measurements at each site was ±10.4%. Thirty-three (33) of these sites were measured under air and 10 sites were measured under deionized water.

RESULTS

Friction Coefficient

We present here the FC data for the SWG and the KD samples; cleaved biotite results are presented in the Data Repository. The AFM samples were collected from fault surfaces of run SWG-1614 (Fig. DR2A), and from run KD-1516 (Fig. DR2B). The FC values vary systematically with orientation and conditions (Fig. 2A; Tables DR1 and DR2). Under room-dry conditions, the unsheared surfaces have μ = 0.64 ± 0.05 for both rock types. On the dolomite surface, the FC slightly dropped to μ = 0.60 ± 0.15 normal to the slickensides. On the granite fault surface, the friction increased to μ = 0.71 ± 0.02 on a rough, sheared surface. The most profound friction decrease was observed parallel to the slickensides: the FC dropped to μ = 0.34 ± 0.08 and μ = 0.52 ± 0.03 for dolomite and granite, respectively. Under wet (water-covered) conditions parallel to slickensides, the friction dropped even further to μ = 0.15 ± 0.05 (dolomite) and μ = 0.31 ± 0.05 (granite).

The above nanoscale FC values are comparable to the macroscopic FC for the host experiments. The AFM-analyzed dolomite surface is from run KD-1516 with stepping slip velocity up to 0.37 m/s, and slip distance of 7.9 m (Fig. 2B; Fig. DR2B). The FC decreased systematically with velocity increase, and reached μ = 0.37 ± 0.02 at the final stage (Fig. 2B); this FC is almost identical to the AFM μ = 0.34 ± 0.08 that was measured room dry and slickenside parallel on the same fault (Fig. 2A). This result was initially puzzling: the glass bead appears as an ideal single asperity, and single-asperity friction is expected to differ from the multi-asperity, Coulomb friction (Byerlee, 1978; Li and Kim,
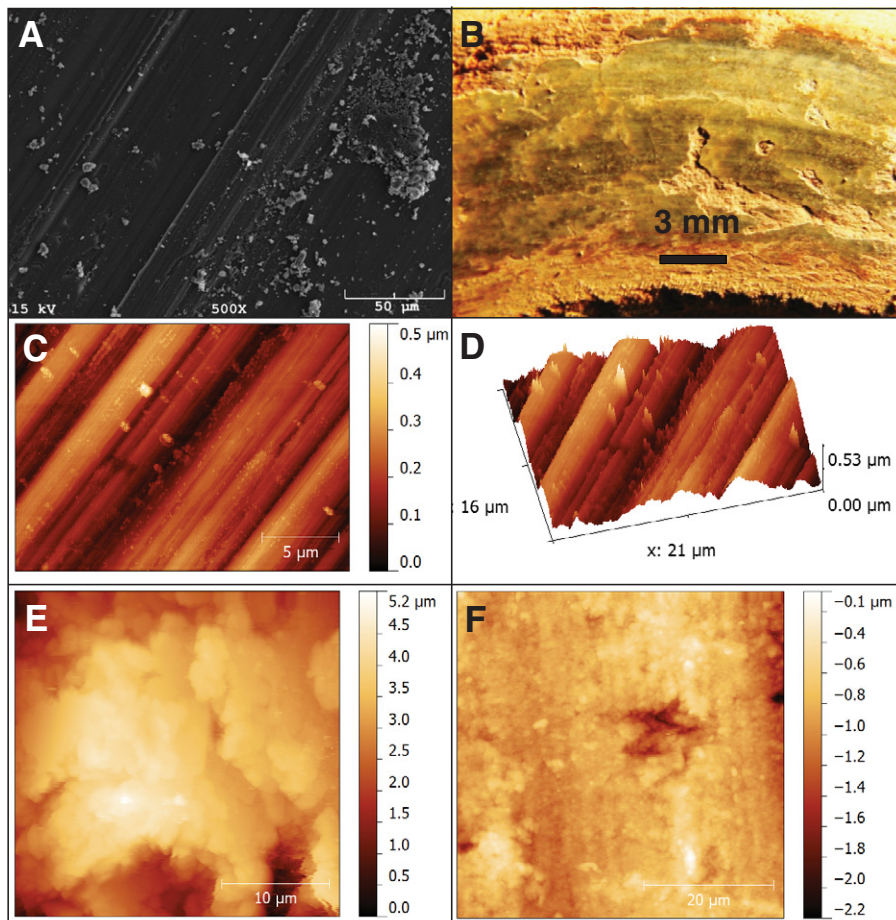
---

*E-mail: reches@ou.edu.

Figure 1. Fault surfaces. A: Scanning electron microscopy image of an experimental fault of Kasota dolomite (KD) from Minnesota, United States. B: Experimental fault surface of KD after run KD-1516 of present study. C: Atomic force microscopy (AFM) image of sheared surface of KD (run KD-1516); note the distinct, clear striations at sub-micron spacing and a few fine grains (elevated bright spots). D: Three-dimensional view of C. E: AFM morphology map of un-sheared KD surface; note irregular, rough surface. F: AFM image of sheared surface of Sierra White granite from California, United States; note the faint slickenside striations in general north-south direction, fine grains, and damage (hole in the center). Gradational color scale next to panels C, E, and F indicate surface elevation in microns.

and normal to striations falls between the two end members.

We further noted systematic changes of the PSD slope, β. The un-sheared profiles have steep PSD curves, with $\beta = 2.3 \pm 0.1$. Profiles measured normal to the striations are smoother, with similar $\beta = 2.4 \pm 0.1$, and profiles measured parallel to the striations are even smoother and with lower $\beta = 1.4 \pm 0.4$. Similar roughness anisotropy between slip-parallel and slip-normal profiles on fault surfaces was observed by Power et al. (1987), Sagy et al. (2007), Renard et al. (2006), and Candela et al. (2011). The reduction of the un-sheared, original slope $\beta > 2$, to $\beta < 2$ (1.4 ± 0.4 in our case) parallel to the slip direction, was previously documented in profilometer measurements of fault surfaces with tens to hundreds of meters of slip (Sagy et al., 2007).

In addition to the above PSD curves, we calculated the RMS roughness along hundreds of 1 µm segments both slip parallel and slip normal. These "micron-scale-RMS" values were calculated for 1 µm segments that are close in size to the AFM friction measurements (0.1–0.25 µm). This scale of roughness calculations was selected because the parameters of Ra or RMS depend on the measurement area (larger areas yield larger Ra and RMS), and thus are valid at the measurement scale. We use the Ra and RMS results in the discussion below.

Friction-Velocity Relations

The above AFM measurements, which were conducted on a few selected fault surfaces, fit the macroscopic observations of an extensive experimental effort (e.g., Reches and Lockner, 2010; Green et al., 2010; Boneh, 2012; Chang et al., 2012). Figure 4 displays the friction-velocity relations in 81 experiments with KD that slipped under constant or stepped velocity (Boneh, 2012). The figure reveals a consistent trend: steady $\mu = 0.8$–0.9 up to a critical velocity, V_C, of ~0.08 m/s, and a rapid drop to $\mu \sim 0.3$ as the velocity approaches 1 m/s. The surfaces of KD that were analyzed here (Figs. 1–3) fit well this trend (blue square, Fig. 4).

A common feature in the dolomite experiments at velocities above V_C is that the fault surfaces were coated, partly or fully, with a hard, smooth, light-reflective crust (Boneh, 2012) that was used for the AFM measurements (Figs. 1A–1D). Under velocities exceeding 0.3 m/s, the two fault surfaces were almost fully coated with this crust without gouge powder (Fig. 1B). The top of this hard crust is a layer ~100 nm thick composed of 10–30-nm-diameter particles (Green et al., 2010) that are similar in size to the typical gouge grains observed in AFM imaging. Finally, during the high-speed experiments in which the crust was formed, the average fault surface temperature exceeded 400 °C (calculated by finite-element modeling of the

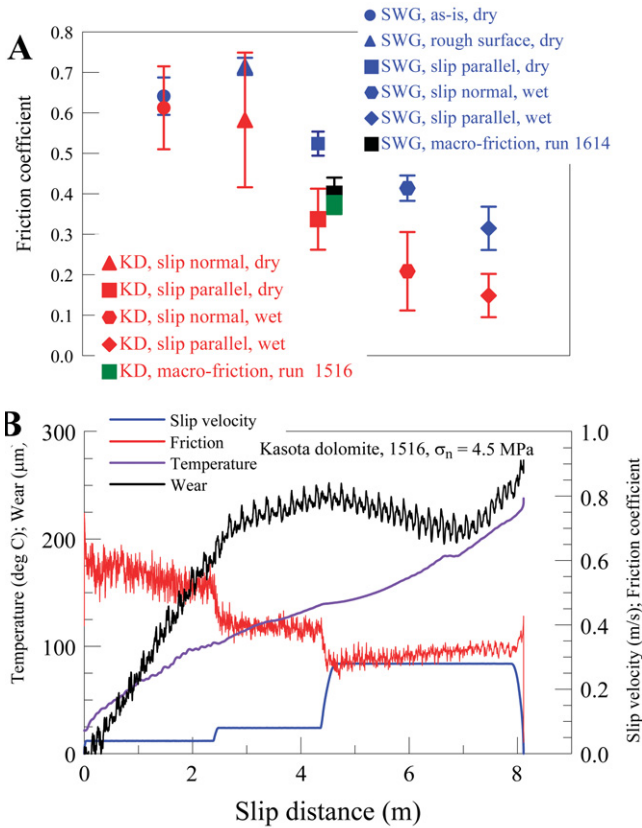2008). However, the AFM profile of the glass bead (Fig. DR3) reveals roughness of 26.7 nm, such that it should be considered a multi-asperity body. Thus, the friction measurements with a multi-asperity glass bead may be considered equivalent to the macroscopic friction, as actually observed (Fig. 2A).

Fault Surface Roughness

We measured the nanoscale morphology of the experimental faults in typical AFM imaging mode with a sharp-tip probe (Figs. 1C–1F). Un-sheared dolomite surfaces showed irregular, rough topography (Fig. 1E). The dolomite fault surfaces that were sheared at high velocity are relatively uniform (Fig. 1B), with prevailing slickenside striations spaced at a fraction of a micron (Figs. 1C and 1D). The granite fault surface displays a heterogeneous range of textures. Parts of it are rough with deep holes and plowing traces, while other parts are weakly

striated (Fig. 1F), or even locally melted. This heterogeneity of the granite surface prevented simple extrapolation of the small-scale AFM measurements to the behavior of the entire macroscopic fault. Thus, the analysis below of friction-roughness relationships focuses on the KD observations.

We measured tens of AFM profiles across the four types of surfaces: cleaved biotite, un-sheared dolomite, and parallel- and normal-to-slickenside striations of the dolomite fault. The roughness of these surfaces can be presented by power spectral density (PSD) (Power and Tullis, 1991), Ra (= mean height differences from a center line), or RMS (root mean square) roughness (= standard deviation of the height differences) (Power and Tullis, 1991). The PSD curves of our data (Fig. 3A) display a clear and expected trend: the cleaved biotite is the smoothest surface, the un-sheared surface is the roughest, and the roughness of profiles parallel

Figure 2. A: Sub-micron friction coefficients (FC) determined with atomic force microscopy (AFM) glass-bead method on experimental fault surfaces of Kasota dolomite (KD; from Minnesota, United States) (run KD-1516) and Sierra White granite (SWG; from California, United States) (run SWG-1614), and macroscopic FC in final stage of these experiments. Horizontal axis is arbitrary; each symbol indicates tens to hundreds of repetitions with standard deviation error bar (see the Data Repository [see footnote 1]). Note FC variations with orientation (normal and parallel to slickensides) and conditions (room dry and wet)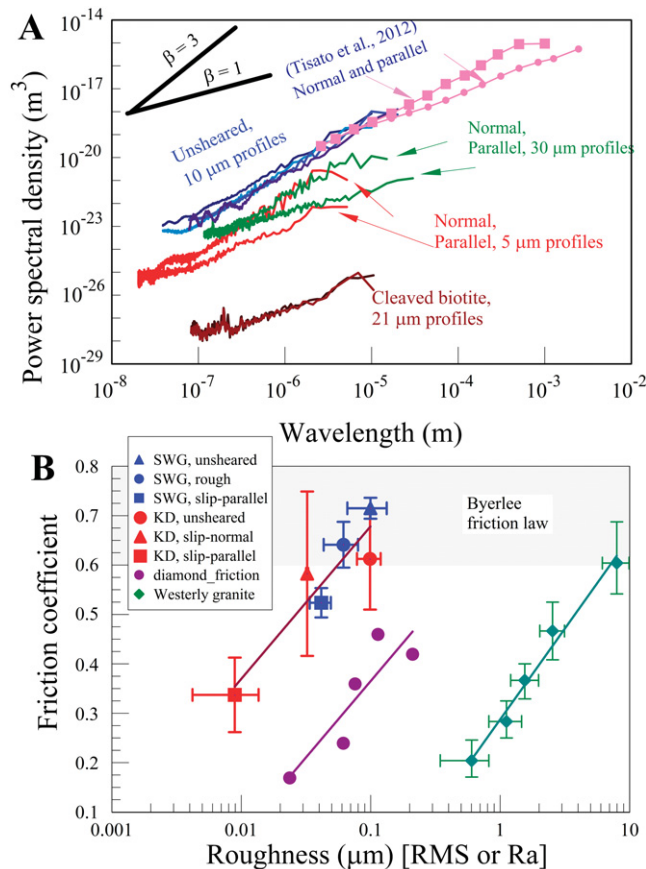. B: History of FC (red), slip velocity (blue), and thermocouple temperature plotted with respect to distance (experiment KD-1516).
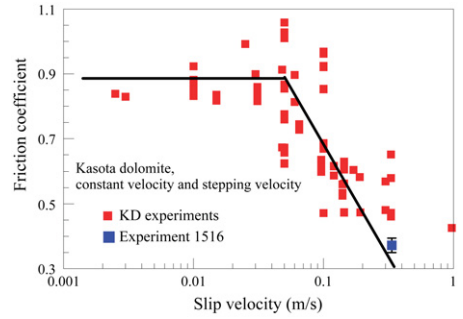

Figure 4. Macroscopic steady-state friction coefficient (FC) and slip velocity of Kasota dolomite from Minnesota, United States. Plot includes 85 data points determined in constant-velocity and stepping-velocity experiments (Reches and Lockner, 2010). Final FC of experiment 1516 (Fig. 2B) is marked by blue square.

thermocouple data). The contribution of these features to fault weakening is discussed below.

DISCUSSION

The main observations of the experimental dolomite faults are: (1) intense dynamic weakening during high-velocity slip (Figs. 2B and 4); (2) formation of a hard, shining surface (Fig. 1B); (3) anisotropic sub-micron friction with lower values parallel to slip striations (Fig. 2A); and (4) anisotropic roughness, with a significantly smoother surface parallel to slip striations (Fig. 3A). These observations led us to a few inferences.

We first discuss the friction-roughness relations following previous observations which showed that smoother surfaces have lower frictional resistance (Byerlee, 1967; Hayward et al., 1992). The AFM friction coefficients in our analysis are plotted as a function of the micron-scale RMS (both friction and roughness measurements at similar scales, above) (Fig. 3B). We also plotted the equivalent relations for Westerly granite from Rhode Island (Byerlee, 1967) and diamond (Hayward et al., 1992). These observations indicate that at length scales of 0.01–10 μm, friction coefficients strongly correlate with roughness RMS (or Ra) with correlation trends of the shape μ = a × ln (RMS or Ra) + b (Fig. 3B). For these rocks (KD, SWG, and Westerly granite) the FC quickly approaches the range of 0.6–0.85, which is the "universal" FC for brittle fault surfaces independently of rock type, velocity, and temperature (Byerlee, 1978). We conclude from these relations that the friction reduction of faults is primarily controlled by smoothing (= roughness reduction) at a scale of 0.01–10 μm, whereas the roughness at larger scales of natural faults has limited effect on the FC. Faults with sub-micron roughness are recognized in the field by their "mirror-like", light-reflecting surfaces (Siman-Tov et al., 2013), and

Figure 3. A: Power spectral density (PSD) of surface roughness of the marked surfaces. PSD data of the present work were calculated for tens of atomic force microscopy (AFM) profiles of the marked length. Note the two end members of cleaved biotite (smoothest) and un-sheared surface (roughest), and roughness difference between striation-parallel and striation-normal roughness. B: Roughness-friction relation at micron scale. Shown are room-dry FC and the AFM roughness of Kasota dolomite (KD; Minnesota, United States) and Sierra White granite (SWG; California, United States) surfaces (roughness as RMS [root mean square] for 1 μm segments), diamond sample A (Hayward et al., 1992), and Westerly granite from Rhode Island, United States (Byerlee, 1967) (roughness as Ra [mean height differences from a center line]). The relations (solid lines) have the form: FC = a ln (roughness) + b, where (a, b) are (0.13, 0.99) for KD-SWG combined, (0.13, 0.67) for diamond A, and (0.16, 0.29) for Westerly granite.

our analysis suggests that such faults slipped under low frictional resistance.

We finally link the main features of high-velocity dolomite faults: they are coated with a smooth, shiny crust (Figs. 1A–1D and 3A) that is composed of ultra-fine grains (Green et al., 2010; Siman-Tov et al., 2013), and which formed under high temperature (>400 °C). We envision that the heated, ultra-fine grains were soft enough to deform plastically, and to form the highly smooth surfaces (RMS < 100 nm for 1 μm profiles; Fig. 3B) with low friction coefficient (Figs. 2 and 4). As these processes occur only at high velocity (V > V$_C$ ~0.08 m/s; Fig. 4), we propose that slip smoothing under high velocity can be an effective mechanism for dynamic weakening during earthquakes. The explicit slip-smoothing mechanism may vary depending on fault composition and slip conditions. For example, dynamic recrystallization (Smith et al., 2012) or asperity abrasion (Byerlee, 1967) facilitate fault surface smoothing and thus could lead to dynamic weakening.

REFERENCES CITED

Attard, P., Stiernstedt, J., and Rutland, M.W., 2007, Measurement of friction coefficient with the atomic force microscope: Journal of Physics: Conference Series, v. 61, p. 51–55, doi:10.1088/1742-6596/61/1/011.

Boneh, Y., 2012, Wear and gouge along faults: Experimental and mechanical analysis [M.S. thesis]: Norman, University of Oklahoma, 72 p.

Byerlee, J.D., 1967, Theory of friction based on brittle fracture: Journal of Applied Physics, v. 38, p. 2928–2934, doi:10.1063/1.1710026.

Byerlee, J.D., 1978, Friction of rocks: Pure and Applied Geophysics, v. 116, p. 615–626, doi:10.1007/BF00876528.

Candela, T., Renard, F., Bouchon, M., Schmittbuhl, J., and Brodsky, E.E., 2011, Stress drop during earthquakes: Effect of fault roughness scaling: Bulletin of the Seismological Society of America, v. 101, p. 2369–2387, doi:10.1785/0120100298.

Carpick, R.W., Agrait, N., Ogletree, D.F., and Salmeron, M., 1996, Variation of the interfacial shear strength and adhesion of a nanometer-sized contact: Langmuir, v. 12, p. 3334–3340, doi:10.1021/la9509007.

Chang, J.C., Lockner, D.A., and Reches, Z., 2012, Rapid acceleration leads to rapid weakening in earthquake-like laboratory experiments: Science, v. 338, p. 101–105, doi:10.1126/science.1221195.

Dieterich, J.H., and Kilgore, B.D., 1994, Direct observation of frictional contacts: New insights for state-dependent properties: Pure and Applied Geophysics, v. 143, p. 283–302, doi:10.1007/BF00874332.

Goldsby, D.L., and Tullis, T.E., 2011, Flash heating leads to low frictional strength of crustal rocks at earthquake slip rates: Science, v. 334, p. 216–218, doi:10.1126/science.1207902.

Green, H.W., Lockner, D.A., Bozhilov, K.N., Madden, A.S., Beeler, N.M., and Reches, Z., 2010, Nanometric gouge in high-speed shearing experiments: Superplasticity?, in Proceedings, American Geophysical Union Fall Meeting 2010, Abstract #T31D–08.

Han, R.H., Shimamoto, T., Ando, J.I., and Ree, J.H., 2007, Seismic slip record in carbonate-bearing fault zones: An insight from high-velocity friction experiments on siderite gouge: Geology, v. 35, p. 1131–1134, doi:10.1130/G24106A.1.

Hayward, I.P., Singer, I.L., and Seitzman, L.E., 1992, Effect of roughness on the friction of diamond on CVD diamond coatings: Wear, v. 157, p. 215–227, doi:10.1016/0043-1648(92)90063-E.

Kosoglu, L.M., Bickmore, B.R., Filz, G.M., and Madden, A.S., 2010, Atomic force microscopy method for measuring smectite coefficient of friction: Clays and Clay Minerals, v. 58, p. 813–820, doi:10.1346/CCMN.2010.0580609.

Li, Q., and Kim, K., 2008, Micromechanics of friction: Effects of nanometer-scale roughness: Proceedings of the Royal Society of London, Series A, v. 464, p. 1319–1343, doi:10.1098/rspa.2007.0364.

Li, Q., Tullis, T.E., Goldsby, D.L., and Carpick, R.W., 2011, Frictional ageing from interfacial bonding and the origins of rate and state friction: Nature, v. 480, p. 233–236, doi:10.1038/nature10589.

Lockner, D.A., and Okubo, P.G., 1983, Measurements of frictional heating in granite: Journal of Geophysical Research, v. 88, p. 4313–4320, doi:10.1029/JB088iB05p04313.

Maurice, P.A., and Lower, S.K., 2008, Use of atomic force microscopy to study soil particle properties and interactions, in Drees, L.R., and Ulery, A.L., eds., Methods of Soil Analysis, Part 5: Mineralogical Methods: Madison, Wisconsin, Soil Science Society of America Book Series 5, p. 299–334.

Mo, Y., Turner, K.T., and Szlufarska, I., 2009, Friction laws at the nanoscale: Nature, v. 457, p. 1116–1119, doi:10.1038/nature07748.

Moore, D.E., and Rymer, M.J., 2007, Talc-bearing serpentinite and the creeping section of the San Andreas fault: Nature, v. 448, p. 795–797, doi:10.1038/nature06064.

Power, W.L., and Tullis, T.E., 1991, Euclidean and fractal models for the description of rock surface roughness: Journal of Geophysical Research, v. 96, p. 415–424, doi:10.1029/90JB02107.

Power, W.L., Tullis, T.E., Brown, S.R., Boitnott, G.N., and Scholz, C.H., 1987, Roughness of natural fault surfaces: Geophysical Research Letters, v. 14, no. 1, p. 29–32, doi:10.1029/GL014i001p00029.

Reches, Z., and Lockner, D.A., 2010, Fault weakening and earthquake instability by powder lubrication: Nature, v. 467, p. 452–455, doi:10.1038/nature09348.

Renard, F., Voisin, C., Marsan, D., and Schmittbuhl, J., 2006, High resolution 3D laser scanner measurements of a strike-slip fault quantify its morphological anisotropy at all scales: Geophysical Research Letters, v. 33, L04305, doi:10.1029/2005GL025038.

Sagy, A., Beodsky, E.E., and Axen, G.J., 2007, Evolution of fault-surface roughness with slip: Geology, v. 35, p. 283–286, doi:10.1130/G23235A.1.

Scholz, C.H., 1998, Earthquakes and friction laws: Nature, v. 391, p. 37–42, doi:10.1038/34097.

Siman-Tov, S., Aharonov, E., Sagy, A., and Emmanuel, S., 2013, Nano-grains form carbonate fault mirrors: Geology, v. 41, doi:10.1130/G34087.1 (in press).

Smith, S.A.F., Di Toro, G., Kim, S., Ree, J.H., Nielsen, S., Billi, A., and Spiess, R., 2012, Co-seismic recrystallization during shallow earthquake slip: Geology, v. 41, p. 63–66, doi:10.1130/G33588.1.

Stiernstedt, J., Rutland, M.W., and Attard, P., 2005, A novel technique for the in situ calibration and measurement of friction with the atomic force microscope: The Review of Scientific Instruments, v. 76, 083710, doi:10.1063/1.2006407.

Tisato, N., Di Toro, G., De Rossi, N., Quaresimin, M., and Candela, T., 2012, Experimental investigation of flash weakening in limestone: Journal of Structural Geology, v. 38, p. 183–199, doi:10.1016/j.jsg.2011.11.017.

Tsutsumi, A., and Shimamoto, T., 1997, High velocity frictional properties of gabbro: Geophysical Research Letters, v. 24, p. 699–702, doi:10.1029/97GL00503.

Tullis, T.E., 1996, Rock friction and its implications for earthquake prediction examined via models of Parkfield earthquakes: Proceedings of the National Academy of Sciences of the United States of America, v. 93, p. 3803–3810, doi:10.1073/pnas.93.9.3803.